Simulation of operation of the multifrequency spaceborne lidar Tektonika-A

G.M. Krekov, M.M. Krekova, and G.G. Matvienko

Institute of Atmospheric Optics,
Siberian Branch of the Russian Academy of Sciences, Tomsk

Received December 6, 1999

The Monte Carlo method is used to model the operation of the multifrequency satellite lidar Tektonika-A, designed for detection of aerosol inversions in the atmospheric boundary layer. Estimates are obtained for the wavelengths λ = 1.06, 0.53, and 0.35 μm (the three harmonics of the Nd:YAG laser) and boundary conditions corresponding to real parameters of the receiving-transmitting lidar system. The basic optical model was chosen to correspond to the background state under the assumption of a stratified inhomogeneity. The model can be generalized to include aerosol inversions of any origin, whether natural or anthropogenic. The obtained results provide information on the dynamic range of the return signal in a given spectral interval for different optical situations. In addition, we determined limiting levels of noise of active origin and caused by outgoing radiation under different optical and geometrical conditions of operation of the lidar system.

Introduction

Aircraft lidar sensing systems have proven to be an efficient tool for solving various applied problems in meteorology, ecology, and atmospheric and oceanic physics.[1,2] When used on orbital stations and research satellites, these systems substantially increase the monitoring capabilities of these facilities, making them global in areal coverage and systematic in character. This is required for real-time monitoring of the spatial fields of the main atmospheric parameters such as, first of all, cloud fields, the altitude structure of aerosol and gaseous components of the troposphere, ecologically dangerous local-scale emissions, etc. At the same time, aircraft lidars hold their place as important instrument facilities in support of satellite observations.

A detailed analysis of the methodological aspects of the problem of laser sensing of the atmosphere from space was made in our early works.[3,4] To date, a number of the early projects have been technically implemented in practice.[5,6] An initial series of measurements by the Russian spaceborne lidar Balkan has already been made. The lidar aboard the orbital station Mir has been operational since August 1995.[7] The Russian–French lidar ALISSA has been in orbit as part of the Priroda unit on the same station since May 1996. In September 1994, a first-of-its-kind, quite successful experiment on multifrequency laser sensing through the total atmospheric depth was performed from onboard the Space Shuttle.[8] Simultaneously, ground-based and aircraft lidar measurements synchronized with this orbital experiment were also made.

Because the results of the first satellite lidar studies of cloud fields, aerosol profiles, and selected surface properties were so encouraging, the next step is to introduce this class of satellite lidars into a system for making continuous monitoring observations of the Earth. Presently, under the auspices of the RSA Etalon program, projects are under way to create a network of small dedicated satellites equipped with detectors of different types (electrical, magnetic, optical, etc.) which can be used for prediction and detection of natural disasters, primarily earthquakes. One precursor of earthquakes is an increased concentration of coarsely dispersed mineral aerosol fraction in the atmospheric boundary layer[9]; therefore, it is planned to equip one of the satellites of this network, namely the Tektonika–A satellite, with a multifrequency lidar capable of making long-term routine measurements.[1]

As is well known, all lidar systems operate under conditions contaminated with noise, including noise of active origin. This last form of noise is created by the lidar signal itself in the course of its multiple interactions with particles of the scattering medium. In the discussion that follows, we present results of a numerical experiment undertaken to study specific features of active optical noise in the receiving system of the given lidar. The calculations are made using the Monte Carlo method, which provides signal estimates with separation into successive orders of multiple scattering and into angular bins of photon entry into the detector. This provides a basis for a detailed analysis of the structure of the return signal as a function of the optical and geometrical conditions of the experiment. Recently, this analysis was made for the lidar Balkan used for sensing cloud fields; the results are presented in Refs. 11–14. The present study expands upon this previous series of works.

Model formulation

The radiative transfer equation was solved for initial and boundary conditions corresponding to the

0235-6880/00/08 677-08 $02.00

operating conditions of a monostatic lidar. It is assumed that the lidar is located at a height H_0 above the surface, while the source emits isotropically into the angular cone $2\pi(1 - \cos\varphi_i)$, where φ_i is the beam divergence. The reflected signal is recorded by a detector whose acceptance cone angle $2\pi(1 - \cos\varphi_d)$ is defined by the detector field-of-view (FOV) angle φ_d. The basic lidar performance specifications required to make model estimates are:

Satellite altitude H_0, km	400–600		
Working wavelengths λ_i, μm	1.064	0.532	0.355
Beam divergence φ_i, mrad	1	0.4	0.4
Pulse duration τ_i, ns	27	27	30
Field of view φ_d, mrad	1–20		
Spatial resolution Δh, km	0.1–1		

The wide field of view (up to 20 mrad) is expected from use of a low-quality multi-element receiving mirror unfolded in space.

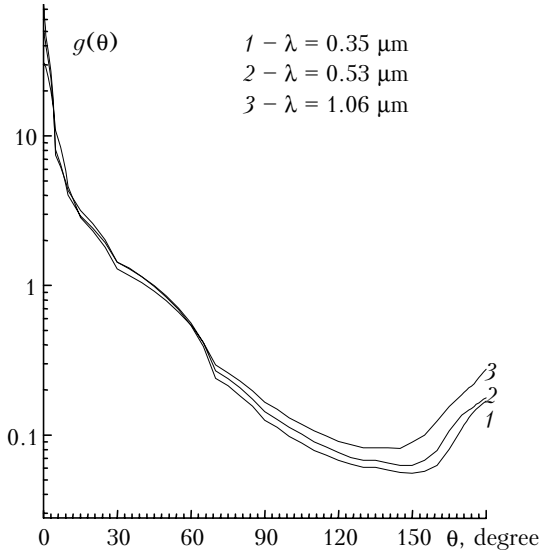

Fig. 1. Angular dependence of the scattering phase function $g(\theta)$ for the given wavelengths.

The algorithm is based on a local estimate; the basic principles of construction of the algorithm are presented in Ref. 15. There is no problem with divergence of this estimate, because the source and detector are located outside the scattering medium. We only note that the mathematical model of the satellite lidar Tektonika-A (see Ref. 1) can be used to study spatiotemporal variations of the optical signal under conditions closely corresponding to actual conditions. This suggests that the multicomponent atmospheric composition can be taken into consideration up to heights $h = 90$ km in the approximation of an inhomogeneous-stratified atmosphere. The optical properties of the scattering medium are described by the scattering phase function $g(\theta)$, extinction coefficient $\sigma(h)$, and single scattering albedo $\Lambda(h)$. Figure 1 presents scattering phase functions calculated for the required wavelengths in accordance with the background model developed by us.[16] This model is based on average values of comprehensive statistical data on the concentration and microphysical properties of the atmospheric aerosol. The results of calculations of different functional dependences are presented in the figures; they are plotted as functions of h, which is equivalent to the accumulated photon path length or the residence time of the photon in the given angular interval in the scattering medium. In addition, $h = ct/2$, where c is the speed of light. Histograms of the functional dependences are plotted for average values over altitude bins $\Delta h = 0.5$ km down to 3 km altitude and over altitude bins $\Delta h = 0.1$ from there on down.

Calculation results

To extract information from laser sensing measurements of the scattering medium, first of all one needs to have a complete picture of the structure of the return signal, which is known to depend both on variations of the optical properties of the medium and on the geometry of the receiving-transmitting system. In addition, one needs to have an estimate of the expected noise level due to multiply scattered radiation in various extreme (from the optical weather standpoint) situations. In this paper we present results of calculations undertaken to address these major lidar-sensing issues. In all of the calculations presented below it was assumed that the lidar is located at a height $H = 400$ km above the Earth's surface.

For convenience of scaling, in all of the figures the time evolution of the relative scalar intensity of the reflected signal is presented for bounded altitude intervals starting from the Earth's surface ($h = 0$ km). Figure 2*a* presents vertical profiles of the extinction coefficient, including contributions from molecular scattering and ozone absorption, while Figures 2*b* and *c* present profiles of backscattered signals $P(h)$ for the working wavelengths of the Nd:YAG laser. These results suggest that problems can arise when recording signals in the IR under conditions of a clear-sky atmosphere. The structure of the $P(h)$ signal is depicted in Fig. 2*c* for two wavelengths, $\lambda = 0.35$ and 1.06 μm. For the aerosol atmosphere in its background state, the reflected signal $P(h)$ at $\lambda = 0.35$ μm is determined almost totally by the molecular scattering component $P_m(h)$. The aerosol component $P_a(h)$ of the signal becomes comparable with the $P_m(h)$ component only in the lower tropospheric layer up to a height of about 0.2 km. As the wavelength λ increases to 1.06 μm, the aerosol component gradually becomes the dominant contributor to $P(h)$, starting from a height of about 4–5 km above the Earth's surface.

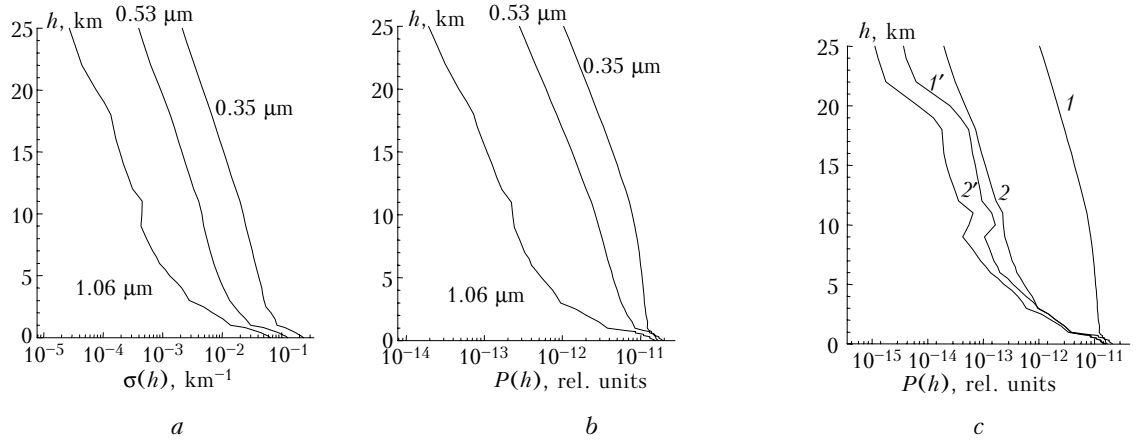

Fig. 2. Altitude profiles of the extinction coefficient $\sigma(h)$ for the utilized laser-sensing wavelengths (*a*); and estimates of the reflected signal $P(h)$ for a lidar with FOV angle φ_d = 10 mrad. Curves *1′* and *2′* show aerosol components $P_a(h)$ of the signal at the wavelengths 0.35 and 1.06 μm, respectively (*b*, *c*).

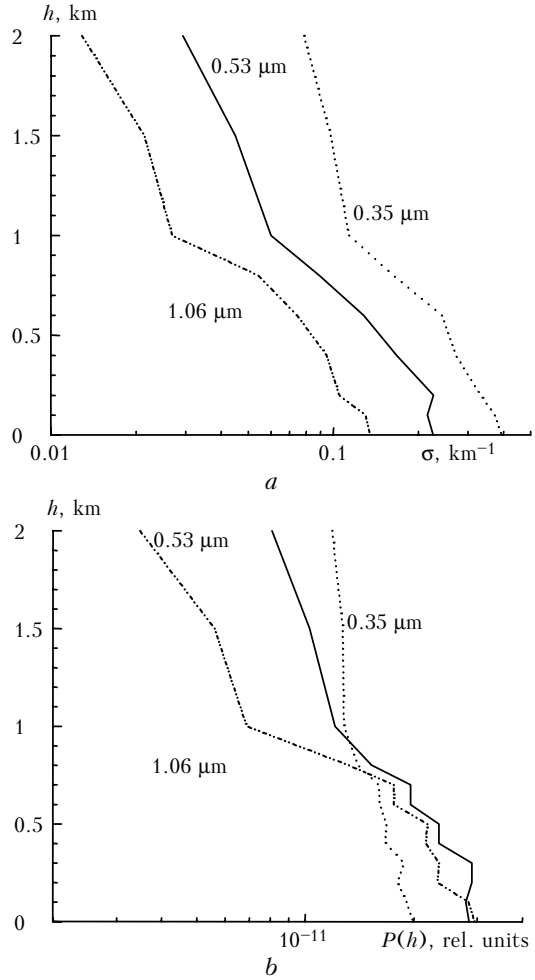

Fig. 3. Numerical modeling results for laser sensing of the atmospheric boundary layer with increased aerosol particle concentration: (*a*) model profiles of the extinction coefficient $\sigma(h)$; and (*b*) altitude profiles of the lidar return $P(h)$ for the given wavelengths. The detector FOV is φ_d = 8.8 mrad.

Potential uses of the satellite lidar system Tektonika-A include detection and, if possible, prediction of natural and anthropogenic disasters accompanied by extreme aerosol emissions in the lower tropospheric layer. In particular, the measurements performed in Guadalahara during the earthquake of October 9, 1995 have shown[9] that several hours before the first shock the number density of the coarsely dispersed aerosol fraction had increased markedly (by a factor of 1.5–2) in the atmospheric boundary layer. The particle composition had modified to include more Si, Ca, and Fe, which is characteristic of minerals emitted from the surface or, perhaps, from deep soil layers. The results of Ref. 9 are unique in some respects but, at the same time, very interesting and were used by us in a numerical experiment. Using these modified aerosol particle size spectra, we recalculated the necessary aerosol scattering characteristics. Also, we assumed that the region of increased tropospheric turbidity extended to an altitude h = 3.5 km.

The corresponding profiles of the extinction coefficient are shown in Fig. 3*a*. Figure 3*b* presents the results of calculations of backscattered signals $P(h)$. It is noteworthy that compared with a non-turbid atmosphere (Fig. 1*b*), in a turbid one we observe not only changes in the strength of the return signals, but also changes in the shapes of the curves calculated for the same wavelengths. It is expected, and the calculated results confirm, that more reliable identification is possible for vertically localized layers of increased turbidity, originating, for example, from burning peat bogs.

In Fig. 4*a*, this situation is mimicked using a ten-times larger aerosol extinction coefficient in a 1-km thick layer at the altitude H = 1 km. The corresponding calculated results are shown in Fig. 4*b*. It is noteworthy that the efficiency of the infrared sensing channel is radically increased in this case. As a result, the spectral behavior of the return signals changes over to the opposite extreme (Fig. 4*c*). This feature, in our opinion, can be used as a qualitative criterion of the existence of anomalous aerosol layers of terrigenous origin.

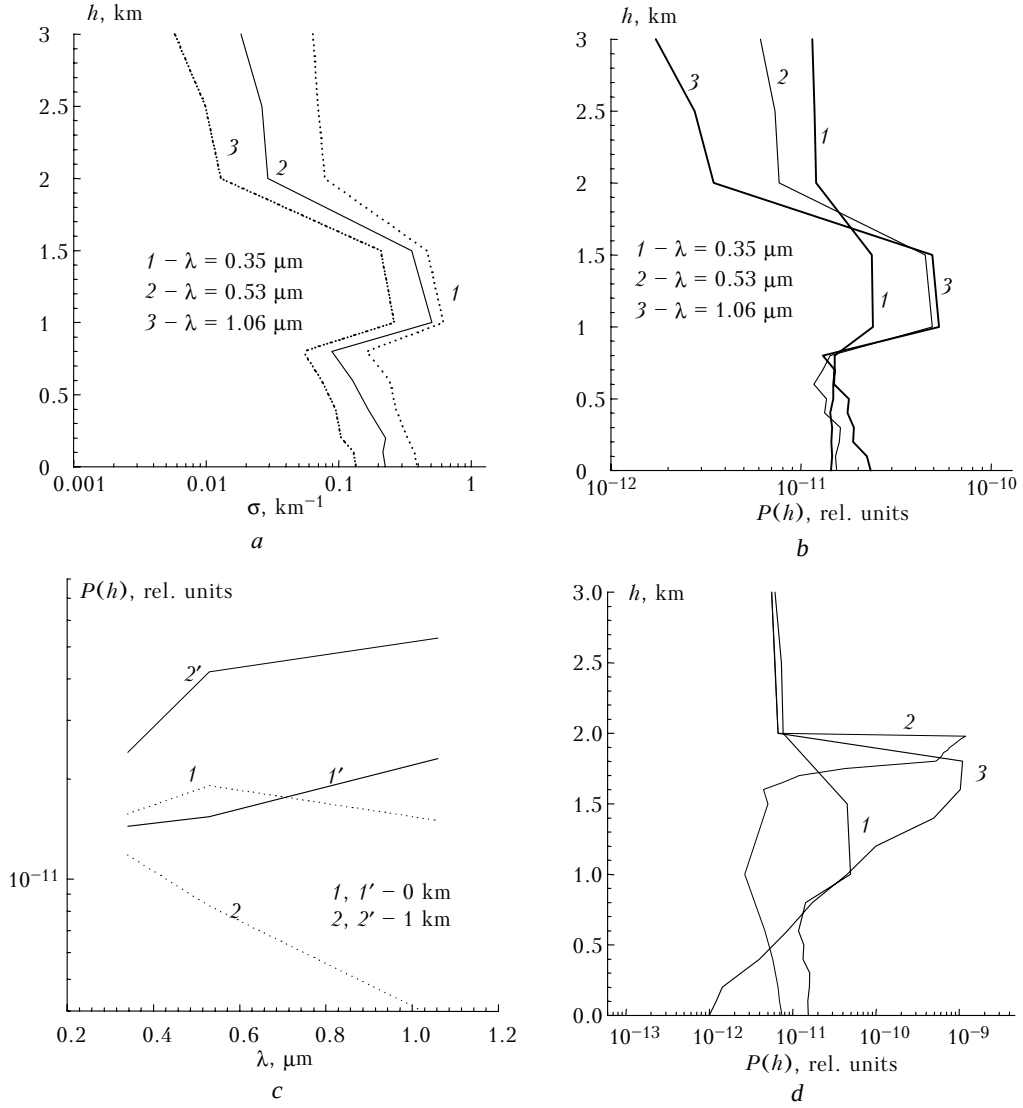

Fig. 4. Results of laser sensing of an aerosol inversion in the near-ground atmosphere: (*a*) model profiles of $\sigma(h)$; (*b*) vertical profiles of $P(h)$; (*c*) spectral behavior of lidar signals returning from different altitude regions located in the inversion zone (curves *2* and *2′*) and outside it (curves *1* and *1′*); and (*d*) comparison of signals reflected from the aerosol inversion region (curve *1*), by a cloud of thickness Δh = 0.2 km (curve *2*), and by a fog layer of thickness Δh = 1 km (curve *3*). Calculations were made for detector FOV φ_d = 8.8 mrad.

In this situation, however, an uncertainty exists about what object the return signal was reflected from: whether it was a low-level cloud or an aerosol inversion. Clouds typically have high optical density. Figure 4*d* compares calculated values of the $P(h)$ signal reflected by cloud, fog, and aerosol inversion layers. The extinction coefficient $\sigma(h)$ for both cloud and fog was taken to be 5 km^{-1}, which is the minimum possible value for liquid droplets in the atmosphere. Our calculations show that the amplitude of the return signal $P(h)$ reflected from a cloud or fog layer is at least two orders of magnitude higher than that of the signal reflected from an aerosol inversion layer even if the optical depth of the latter is increased by a factor of two to three. In addition, the spectral dependence of the signal $P(h)$ reflected by a liquid-droplet aerosol is practically neutral. This is because the scattering phase function $g(\pi)$ changes little in the given spectral interval and, moreover, because, as shown in Refs. 11 and 17, in the satellite sensing scheme the shape of the scattering phase function does not substantially influence the characteristics of the return signal. It may be expected, furthermore, that the polarization characteristics of a lidar signal backscattered by liquid droplets and by mineral particles will differ markedly. However, in the context of satellite sensing applications this issue requires further study.

The receiving system of this multifrequency lidar has a wide (up to 20 mrad) field of view; and this uniqueness of construction dictates that the noise due to multiply scattered radiation be estimated with especial accuracy under various possible conditions including limiting cases. It is this multiple-scattering noise that reduces the information content of laser sensing channels,

thereby decreasing the possibility of obtaining reliable quantitative data on the parameters of the atmosphere. Exact calculations of signals from the troposphere in the absence of clouds are illustrated in Fig. 5. These results are presented in the form of the altitude dependence of the relative contribution of multiple scattering $Pm(h)$ to the total signal $P(h)$. The value of this function depends primarily on the optical density of the medium but also the boundary conditions of the experiment. Figure 5*a* plots the ratio $Pm(h)/P(h)$ calculated for different optical conditions of the atmospheric aerosol, $\lambda = 0.53$ μm, and detector FOV $\varphi_d = 10$ mrad.

Profiles of the extinction coefficient $\sigma(h)$ corresponding to curves *1*, *2*, and *3* are shown in Figs. 2*a*, 3*a*, and 4*a*, respectively; they were calculated for a 30-km thick atmospheric layer with optical depths $\tau \approx 0.175$, 0.25, and 0.75, respectively. As can be seen, even a slight increase in the atmospheric optical depth leads to a considerable growth of the contribution of the $Pm(h)$ component to the signal reflected by the atmospheric boundary layer. The contribution of the background component increases rapidly and becomes dominant for the signals returned from the aerosol inversion layer, and remains so above the inversion layer, all the way up to the top end of the sensing path. It should be noted that the signals from the middle atmosphere (when sensed at nadir) are well described using the single scattering approximation over the entire spectral interval of interest here.

The dependence of the ratio $Pm(h)/P(h)$ on the angular characteristics of the detector is plotted in Fig. 5*b*; it is calculated for the wavelength $\lambda = 0.35$ μm and return signals coming from different altitude bins of the sensing path. In these calculations, we used an aerosol model corresponding to a moderately turbid boundary layer as depicted in Fig. 3*a*; nevertheless, for the UV sensing channel, the optical density of the medium was somewhat higher. It can be seen that as the detector FOV angle increases to $\varphi_d \approx 10$ mrad, the contribution of the background component to the return signal first increases rapidly and then nearly levels off. Thus, a kind of signal saturation takes place, namely the contribution of the background multiply-scattered component becomes increasingly less significant with increasing order of multiple scattering. This feature is not new and is most clearly manifested in satellite sensing applications.

It should be noted that for laser sensing of remote polydispersions, different sensing schemes can be used; and for each it is always possible to theoretically estimate a limiting FOV angle $\varphi_d^{(n)}$ for which the signal amplitude nearly levels off, so that the use of FOV angles $\varphi_d > \varphi_d^{(n)}$ is meaningless.

In multifrequency laser sensing applications, it is also important to remember that the background multiply-scattered component has a spectral dependence. Figure 5*c* plots the ratio $Pm(h)/P(h)$ calculated for a moderately turbid atmosphere in which the profile of $\sigma(h)$ is as shown in Fig. 3*a*; the calculations were performed for two detector FOVs: $\varphi_d = 2.5$ and 10 mrad. The level of $Pm(h)$ is highest in the UV spectral range, where, due to the large value of the scattering phase function $g(\pi)$, molecular scattering is relatively important. In the context of satellite sensing of an aerosol atmosphere, the shape of the scattering phase function has little influence on the level of the background signal component. This follows from calculations of the spectral dependence of $Pm(h)/P(h)$ which assume no molecular scattering and identical optical density of the medium. In this situation, this ratio varies little with wavelength, while the difference in the signal level arises only as a result of the dependence of the scattering phase function $g(\pi)$ on the wavelength.

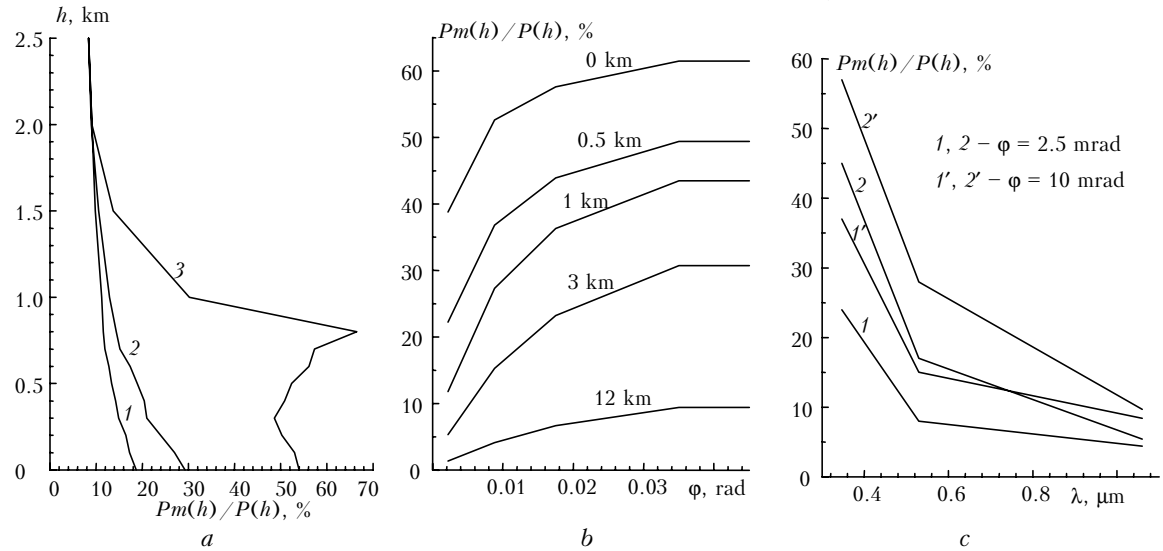

Fig. 5. Dependence of the ratio of the background signal component $Pm(h)$ to the total signal $P(h)$ on the optical and geometrical conditions of the experiment: (*a*) on the optical density of the medium at the wavelength $\lambda = 0.53$ μm; (*b*) on the detector FOV φ_d for different segments of the sensing path and for the wavelength $\lambda = 0.53$ μm; and (*c*) on the wavelength of the radiation source.

Another important factor limiting the utility of a satellite lidar for real-time monitoring of aerosol anomalies in the lower troposphere is the presence of cirrus clouds, which constantly cover a considerable portion of air basin of the planet. Cirrus clouds have small optical depth and, as such, they can lead to an incorrect interpretation of lidar returns or even distort the useful signal coming from the subcloud aerosol layer. Figure 6 illustrates that multiple-scattering noise can be increased by the presence of cloud layers in the altitude interval h = 5.5–7 km relative to the clear-sky value (see Fig. 2*a*). Radiation multiply scattered by clouds contributes to the signal reflected by the subcloud aerosol layer.

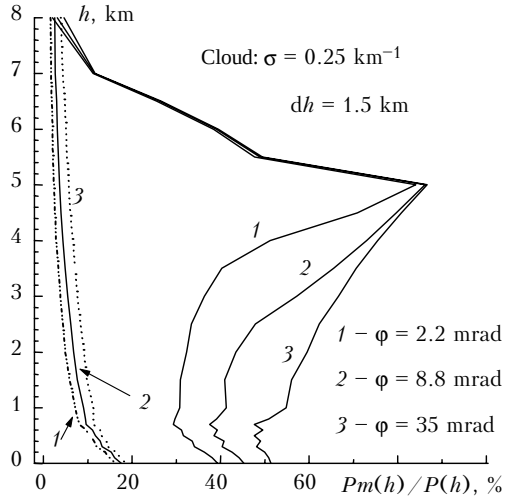

Fig. 6. Influence of cirrus clouds with optical depth $\tau = 0.5$ on the multiple-scattering background component; curves *1* through *3* on the left side correspond to conditions of the "background" atmospheric state.

The obtained model estimates allow us to address one more methodological aspect of the utility of approximate estimates for retrieval of optical properties of the medium from lidar returns. Figure 7 plots the total backscattered signal separated into orders of multiple scattering at three wavelengths. The numbers alongside the curves correspond to the orders of multiple scattering. The case of a weakly turbid atmosphere is considered. As can be seen, in the case of a clear or weakly turbid atmosphere, in the near-IR the inverse problem can be solved with good accuracy taking just two multiple-scattering orders into account. The situation is more complex in the UV spectral range where at least three orders of multiple scattering must be taken into account. Rephrasing the above-said, the UV sensing data can be used in atmospheric sensing applications as reference data for selection of the molecular scattering component.

The validity of the results presented here is confirmed by numerous tests of our model estimates against the results of field experiments (see, e.g., Refs. 17 and 18). In addition, they have been successfully used to develop measurement data interpretation techniques (see, e.g., Ref. 19).

Our analysis would not be complete without addressing the issue of how the potential capabilities of satellite lidars are restricted by noise caused by background radiation of the atmosphere–surface system. This background radiation has many sources, the most powerful of which being the Sun with the Moon, stars, and sensed objects (such as clouds), among others, being much weaker.

In many cases, the background radiation can be approximated by Planck's law, i.e., it can be represented as the emission of an ideal blackbody with temperature T_s. In accordance with this law, for unpolarized radiation the spectral intensity $W(\lambda)$ emitted in the spectral region $(\lambda, \lambda + d\lambda)$ by a surface of unit area into a hemisphere has the form

$$W(\lambda)\, d\lambda = 2\pi c^2\, h\Delta\lambda/\lambda^5\, [\exp(hc/\lambda k T_s) - 1],$$

where c is the speed of light, and h and k are the Planck and Boltzmann constants.

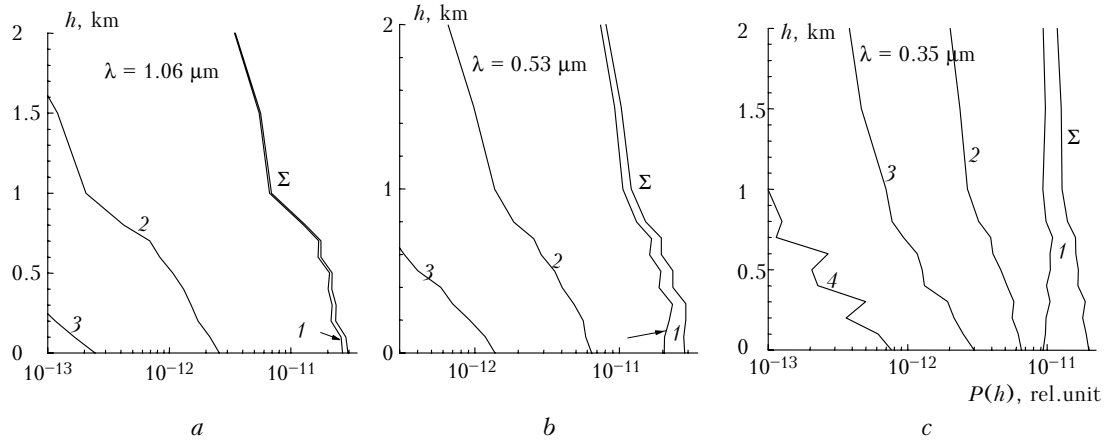

Fig. 7. Decomposition of the signal $P(h)$ into scattering orders for the given wavelengths (the numbers alongside the curves correspond to the orders of multiple scattering). The FOV angle $\varphi_d = 8.8$ mrad. The label Σ denotes the total signal.

Specific features of the background solar radiation in an aerosol atmosphere have been studied in sufficient detail. A detailed analysis of available engineering methods of estimating the brightness of outgoing radiation $B_A(\lambda)$ in the visible wavelength range was made by Smerkalov in his monograph.[20]

For the lidar system Tektonika-A we employ Monte Carlo estimates of the background solar radiation. As was noted above, with the Monte Carlo method it is possible to account for complex boundary conditions and to use a realistic atmospheric model. The main factors determining the background level in the lidar receiving system are the solar zenith angle $Z_\odot$ and the aperture area S and FOV angle φ_d of the receiving mirror. Figure 8 plots the dependence of the power of the background signal P_A on the solar zenith angle $Z_\odot$ for the two sensing wavelengths 0.35 and 0.53 μm, FOV angle $\varphi_d = 1.5$ mrad, and area of the receiving mirror $S = 2$ m^2.

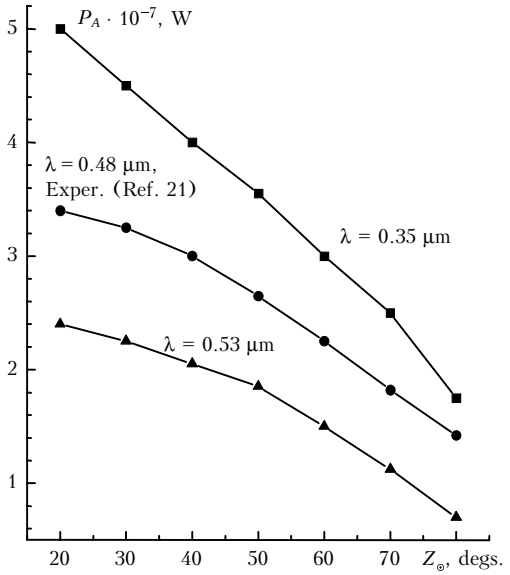

Fig. 8. Influence of the solar zenith angle on the power level of the outgoing radiation.

Qualitative and quantitative consistency of the obtained results is verified by comparison with results of direct satellite observations,[21] recalculated to account for the parameters of the given lidar. In Fig. 9, P_A is plotted versus FOV angle φ_d. As can be seen, the level of background noise increases as the square of the FOV angle φ_d.

Generally, even for small FOV angles (1–3 mrad), the power of the background radiation under daytime conditions is comparable with that of the useful signal because, given the lidar system parameters indicated above and the nominal pulse energy at the wavelengths $\lambda = 0.35$ and 0.53 μm, the variations of the power of the useful signal $P(h)$ typically lie in the dynamic range $10^{-9} \le P(h) \le 10^{-7}$ W. This fact, though known from early satellite experiments, impedes reliable retrieval of the optical characteristics of aerosol scattering using present-day, low-energy, small-size lidar capabilities.

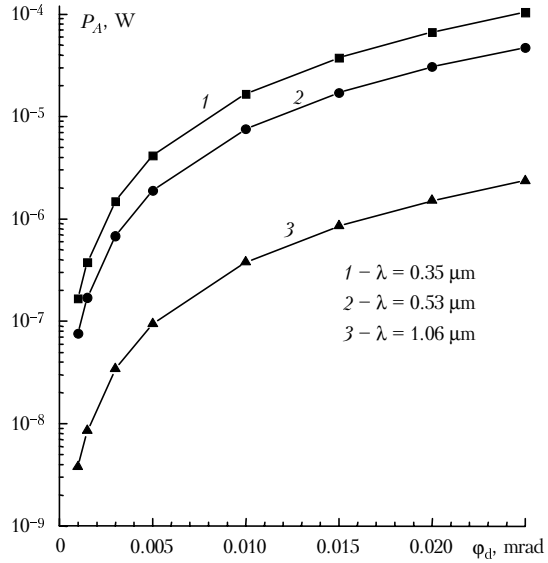

Fig. 9. Dependence of the power level of the background component of the lidar signal (caused by outgoing radiation) on the detector FOV angle.

On the other hand, according to current estimates (see, e.g., Ref. 22), the background radiation of the nighttime sky can be safely neglected for the class of problems of concern here. Even under conditions of a full Moon, the brightness of the nighttime sky in the nadir direction at visible wavelengths is several orders of magnitude lower than the level of the useful signal backscattered by aerosol.

In summary, the obtained results indicate that the multifrequency lidar considered here is capable of detecting aerosol anomalies in the lower atmosphere on the dark side of the planet. Under these conditions, it is possible to use a receiving mirror with a wide field of view (up to $\varphi_d \approx 20$ mrad) because the signal saturates for a much smaller field of view $\varphi_d^{(n)}$, and, hence, this will not produce an additional increase in the contribution of the multiple-scattering noise.

References

1. B.M. Morley, K.K. Laursen, L.F. Radke, and A.D. Clarke, in: *International Airborne Remote Sensing Conference and Exhibition*, 24–27 June 1996, San Francisco, California USA.
2. V.S. Shamanaev, Atmos. Oceanic Opt. **6**, No. 2, 101–103 (1993).
3. V.E. Zuev, G.M. Krekov, and I.E. Naats, Acta Astronautica **1**, 93–103 (1974).
4. V.M. Zakharov, ed., *Laser Sensing of the Atmosphere from Space* (Gidrometeoizdat, Leningrad, 1988), 213 pp.
5. Y.S. Balin, V.V. Burkov, I.V. Znamenskii, et al., in: *Abstracts of Reports at 15th International Laser Radar Conference*, Tomsk (1990), pp. 12–13.
6. M.P. McCormick , D.M. Winker, E.V. Browell, Bull. Meteorol. Soc. **74**, 205–214 (1993).

7. Yu.S. Balin, A.A. Tikhomirov, and S.V. Samoilova, Atmos. Oceanic Opt. **10**, No. 3, 209–220 (1997).
8. W. Renger, C. Kieme, H.-G. Schreiber, M. Wirth, and P. Moerl, *Final Results Workshop Proc.* (IROE-CNR, Florence, Italy, 1995), pp. 15–19.
9. L.S. Ivlev, V.I. Davydova, O.A. Vargas, and A. Martinez, Atmos. Oceanic Opt. **11**, No. 5, 428–431 (1998).
10. G.G. Matvienko, G.P. Kokhanenko, V.S. Shamanaev, and V.A. Alekseev, in: *Abstracts of Reports at Intern. Symposium on Remote Sensing* (Barcelona, 1998), pp. 37–38.
11. G.M. Krekov, and M.M. Krekova, Atmos. Oceanic Opt. **11**, No. 1, 42–49 (1998).
12. V.E. Zuev, G.M. Krekov, M.M. Krekova, and G.A. Titov, Appl. Opt. **26**, No. 15, 3018–3025 (1987).
13. M.M. Krekova, Atmos. Oceanic Opt. **12**, No. 4, 362–367 (1999).
14. G.M. Krekov, M.M. Krekova, and V.S. Shamanaev, Appl. Opt. **37**, No. 9, 1589–1601 (1998).
15. G.I. Marchuk, G.A. Mikhailov, M.A. Nazaraliev, et al., *Monte Carlo Method in Atmospheric Optics* (Nauka, Novosibirsk, 1976).
16. V.E. Zuev and G.M. Krekov, *Optical Models of the Atmosphere* (Gidrometeoizdat, Leningrad, 1986), 256 pp.
17. G.M. Krekov, M.M. Krekova, and I.V. Samokhvalov, Issled. Zemli iz Kosmosa, No. 6, 77–83 (1986).
18. G.M. Krekov, S.I. Kavkyanov, and M.M. Krekova, *Interpretation of Signals of Optical Sensing of the Atmosphere* (Nauka, Novosibirsk, 1987), 185 pp.
19. S.V. Samoilova, Yu.S. Balin, and M.M. Krekova, Atmos. Oceanic Opt. **11**, No. 1, 50–55 (1998).
20. V.A. Smerkalov, *Applied Atmospheric Optics* (Gidrometeoizdat, St. Petersburg, 1997), 335 pp.
21. A.G. Laktionov, N.A. Lutseva, V.A. Mironenko, and V.S. Suetin, Atm. Opt. **4**, No. 1, 86–88 (1991).
22. V.K. Pratt, *Laser Communication Systems* (Svyaz', Leningrad, 1972), 232 pp.